Acetyl-CoA carboxylase inhibition by ND-630 reduces hepatic steatosis, improves insulin sensitivity, and modulates dyslipidemia in rats

Geraldine Harriman[a], Jeremy Greenwood[b], Sathesh Bhat[b], Xinyi Huang[c], Ruiying Wang[d], Debamita Paul[d], Liang Tong[d], Asish K. Saha[e], William F. Westlin[a], Rosana Kapeller[a], and H. James Harwood Jr.[a,1]

[a]Nimbus Therapeutics, Cambridge, MA 02141; [b]Schrodinger Inc., New York, NY 10036; [c]Pharmaron Beijing Co. Ltd., Beijing 100176, China; [d]Department of Biological Sciences, Columbia University, New York, NY 10027; and [e]Department of Medicine and Physiology, School of Medicine, Endocrinology, Diabetes, and Nutrition, Boston University, Boston, MA 02118

Edited by Rab K. Prinjha, GlaxoSmithKline, United Kingdom, and accepted by the Editorial Board January 11, 2016 (received for review October 19, 2015)

Simultaneous inhibition of the acetyl-CoA carboxylase (ACC) isozymes ACC1 and ACC2 results in concomitant inhibition of fatty acid synthesis and stimulation of fatty acid oxidation and may favorably affect the morbidity and mortality associated with obesity, diabetes, and fatty liver disease. Using structure-based drug design, we have identified a series of potent allosteric protein–protein interaction inhibitors, exemplified by ND-630, that interact within the ACC phosphopeptide acceptor and dimerization site to prevent dimerization and inhibit the enzymatic activity of both ACC isozymes, reduce fatty acid synthesis and stimulate fatty acid oxidation in cultured cells and in animals, and exhibit favorable drug-like properties. When administered chronically to rats with diet-induced obesity, ND-630 reduces hepatic steatosis, improves insulin sensitivity, reduces weight gain without affecting food intake, and favorably affects dyslipidemia. When administered chronically to Zucker diabetic fatty rats, ND-630 reduces hepatic steatosis, improves glucose-stimulated insulin secretion, and reduces hemoglobin A1c (0.9% reduction). Together, these data suggest that ACC inhibition by representatives of this series may be useful in treating a variety of metabolic disorders, including metabolic syndrome, type 2 diabetes mellitus, and fatty liver disease.

acetyl-CoA carboxylase | enzyme inhibition | fatty liver disease

Fatty acid metabolism dysregulated through elevated fatty acid synthesis (FASyn), impaired fatty acid oxidation (FAOxn), or both is a hallmark of various metabolic disorders, including insulin resistance, hepatic steatosis, dyslipidemia, obesity, metabolic syndrome (MetSyn), and nonalcoholic fatty liver disease (NAFLD), that can lead to the development of type 2 diabetes (T2DM), nonalcoholic steatohepatitis (NASH), and atherosclerotic vascular disease (1–6). Altered fatty acid metabolism also is a hallmark of cancer and contributes to the abnormal and sustained cellular proliferation of malignancy (7, 8). Therefore inhibition of FASyn and/or stimulation of FAOxn have the potential to affect these maladies favorably.

As a result of its unique position in intermediary metabolism, pharmacologic inhibition of acetyl-CoA carboxylase (ACC) offers an attractive modality for limiting FASyn in lipogenic tissues while simultaneously stimulating FAOxn in oxidative tissues (1, 9). ACC catalyzes the ATP-dependent carboxylation of acetyl-CoA to form malonyl-CoA, the rate-limiting and first committed reaction in FASyn (1, 9–11). This conversion proceeds in two half-reactions, a biotin carboxylase (BC) reaction and a carboxyltransferase (CT) reaction (1, 9–11). ACC activity is tightly regulated through a variety of dietary, hormonal, and other physiological responses including feed-forward activation by citrate, feedback inhibition by long-chain fatty acids, reversible phosphorylation and inactivation by AMP-activated protein kinase (AMPK), and modulation of enzyme production through altered gene expression (1, 9–12).

ACC exists as two tissue-specific isozymes that are encoded by separate genes and display distinct cellular distributions (10, 13, 14). ACC1 is a cytosolic enzyme present in lipogenic tissues (liver, adipose); ACC2 is a mitochondrially associated isozyme present in oxidative tissues (liver, heart, skeletal muscle) (10, 15). In the liver, malonyl-CoA formed in the cytoplasm by ACC1 is used primarily for FASyn and elongation (1), whereas malonyl-CoA formed at the mitochondrial surface by ACC2 acts primarily to regulate mitochondrial FAOxn (1) through allosteric inhibition of carnitine palmitoyltransferase-1 (16). This functional compartmentalization results from a combination of synthesis proximity and the rapid action of malonyl-CoA decarboxylase (1). In the heart and skeletal muscle, which lack ACC1 and thus have a limited capacity for FASyn, the malonyl-CoA formed by ACC2 functions primarily to regulate FAOxn (1). Adipose tissue primarily contains ACC1 to support FASyn in that tissue (1).

Over the past two decades numerous lines of evidence have emerged that strongly support the concept that direct inhibition of ACC is an important therapeutic target. Initial studies with the long-chain fatty acid analog 5-(tetradecyloxy)-2-furancarboxylic acid (17, 18) and the isozyme-nonselective, active site-directed ACC inhibitor CP-640186 (1, 19) have demonstrated the potential for direct ACC inhibition to affect favorably a plethora of metabolic disorders. These pharmacologic studies have been supported further through genetic manipulation of ACC, including studies with ACC2-knockout mice (20, 21), ACC antisense oligonucleotides (22), TRB3 transgenic mice that have increased rates of ACC

Significance

Using structure-based drug design, we have identified a series of potent allosteric protein–protein interaction acetyl-CoA carboxylase inhibitors, exemplified by ND-630, that interact within the acetyl-CoA carboxylase subunit phosphopeptide acceptor and dimerization site to prevent dimerization and inhibit enzymatic activity. ND-630 reduces fatty acid synthesis and stimulates fatty acid oxidation in cultured cells and experimental animals, reduces hepatic steatosis, improves insulin sensitivity, reduces weight gain without affecting food intake, and favorably affects dyslipidemia in diet-induced obese rats and reduces hepatic steatosis, improves glucose-stimulated insulin secretion, and reduces hemoglobin A1c in Zucker diabetic fatty rats. These data suggest that ND-630 may be useful in treating a variety of metabolic disorders, including metabolic syndrome, type 2 diabetes, and fatty liver disease.

Author contributions: G.H., J.G., L.T., W.F.W., R.K., and H.J.H. designed research; J.G., S.B., X.H., R.W., D.P., and A.K.S. performed research; X.H. contributed new reagents/analytic tools; G.H., J.G., S.B., X.H., L.T., A.K.S., W.F.W., R.K., and H.J.H. analyzed data; and H.J.H. wrote the paper.

Conflict of interest statement: G.H., J.G., S.B., W.F.W., R.K., and H.J.H. have filed patents that contain ND-630 and related analogs.

This article is a PNAS Direct Submission. R.K.P. is a guest editor invited by the Editorial Board.

Freely available online through the PNAS open access option.

[1]To whom correspondence should be addressed. Email: h.james.harwood@gmail.com.

This article contains supporting information online at www.pnas.org/lookup/suppl/doi:10.1073/pnas.1520686113/-/DCSupplemental.

degradation (23), and mice with alanine-knockin mutations in the AMPK phosphorylation sites on ACC1 and ACC2 that render them constitutively active (24). Furthermore, studies with combined ACC1 and ACC2 antisense oligonucleotides (22) and with isozyme-specific and/or tissue-specific ACC-knockout mice (25, 26) have provided strong evidence that dual inhibition of ACC1 and ACC2 is superior to the inhibition of either isozyme alone.

A large number of isozyme-nonselective ACC inhibitors have been identified that interfere directly with ACC catalysis through interaction within the CT domain of the enzyme and have been shown to be potent in vitro and efficacious in vivo (1, 9, 19, 27–30). Indeed, in early clinical trials one such inhibitor recently has been shown to reduce FASyn and to stimulate FAOxn after a single oral dose (29). However, the regions of the enzyme to which these inhibitors interact are very hydrophobic (9, 11, 31–33), and thus these inhibitors lack optimal pharmaceutical properties. In contrast, the dimerization site of the enzyme, located on the BC domain, is a shallow, hydrophilic pocket that is the site to which both the phosphopeptide of ACC that is phosphorylated by AMPK and the natural products fungicide soraphens bind to prevent dimerization and inhibit enzymatic activity (9, 34–36). We therefore hypothesized that an allosteric inhibitor that binds to this region of the enzyme would exhibit superior physicochemical properties, would be highly selective relative to other carboxylases because this site is not conserved among the mammalian carboxylases (37), and would mimic the physiological inhibition of ACC by AMPK.

In this report, we describe use of structure-based drug design (SBDD) to identify a unique series of potent and efficacious allosteric protein–protein interaction inhibitors that interact within the ACC subunit dimerization and phosphopeptide acceptor site to prevent dimerization and inhibit the enzymatic activity of both ACC isozymes. We also demonstrate that ND-630, a representative analog of this series that exhibits favorable pharmaceutical properties, is highly effective in reducing hepatic steatosis, improving insulin sensitivity, and favorably affecting dyslipidemia in rats with diet-induced obesity (DIO) and in Zucker diabetic fatty (ZDF) rats, suggesting its utility in treating a variety of metabolic disorders.

Results

Discovery of ND-630. To identify isozyme-nonselective inhibitors that interact within the phosphopeptide acceptor and dimerization site on the BC domain of the enzyme to prevent dimerization and inhibit enzymatic activity, we used the crystal structure of human ACC2 BC domain (hACC2 BC) complexed with Soraphen A [Research Collaboratory for Structural Bioinformatics (RCSB) ID code 3GID], together with a Glide-based Virtual Screening Workflow guided by insights from WaterMap, as outlined in *Materials and Methods*. Using this technology, we identified chemical structures possessing high probability-of-success scores for binding to this site based on their potential for forming hydrogen bonds, electrostatic interactions, and hydrophobic interactions with key amino acid residues and for displacing high-energy water molecules within this dimerization site.

Based on this modeling, a set of 250 diverse structures with high probability-of-success scores were identified through virtual screening and subsequently were evaluated for their ability to inhibit hACC1 and hACC2, using saturating substrate concentrations to minimize the identification of inhibitors that interact within the active center. From these evaluations we identified several distinct structures that inhibited both hACC isozymes through interactions that, based on substrate kinetic analyses, were not within the catalytic center. One of these inhibitors, ND-022 (hACC1 IC_{50} 3.9 μM; hACC2 IC_{50} 6.6 μM) (Fig. 1*A*), was shown to interact within the dimerization site by displacing fluorescently labeled Soraphen A from hACC2 BC (Fig. 1*B*) and by overlapping binding sites for ND-022 and Soraphen A in cocrystal structures with hACC2 BC (Fig. 1*D*). These observations were corroborated by comparative analyses of the thermal stability of hACC2 BC when complexed with Soraphen A and ND-022 (Fig. 1*C*).

Using SBDD tools, including WaterMap and Prime/MM-GBSA, together with the crystal structure of ND-022 complexed with hACC2 BC, we modified the chemical structure of ND-022, as outlined in *Materials and Methods*, to optimize noncovalent interactions with dimerization site amino acid residues and to maximize the displacement of high-energy water molecules within this site while simultaneously incorporating structural elements to impart favorable drug-like properties. This strategy led to the identification of ND-630 (Fig. 2*A*), whose affinity and pharmacokinetic properties are summarized in Table S1.

Inhibition of hACC1 and hACC2 by ND-630. ND-630 inhibited hACC1 with an IC_{50} of 2.1 ± 0.2 nM (values are given as mean ± SEM unless otherwise stated) ($n = 7$) and hACC2 with an IC_{50} of 6.1 ± 0.8 nM ($n = 15$) (Fig. 2*B*). Inhibition was reversible and highly specific for ACC, as evidenced by the absence of an effect of ND-630 on the activity of 101 enzymes, receptors, growth factors, transporters, and ion channels of the Ricerca DrugMatrix Panel (https://www.eurofinspanlabs.com) at 10 μM (Table S2). In addition, because the ACC dimerization site is not conserved among the mammalian carboxylases (37), ND-630 lacks the ability to inhibit any of these mechanistically related enzymes and therefore exhibits absolute specificity for ACC inhibition relative to other mammalian carboxylases.

Mechanism of ACC Inhibition by ND-630. As anticipated, based on the premise that led to its identification, ND-630 inhibits ACC activity by interacting within the phosphopeptide-acceptor and dimerization site of the enzyme to prevent dimerization. This interaction is exemplified by the structure of ND-630, modeled into the crystal structure of ND-646 (the primary amide of ND-630) complexed with hACC2 BC at 2.6-Å resolution (Fig. 2*C*). Like Soraphen A, ND-630 interacts within the dimerization site of the enzyme with the same residues as the AMPK-phosphorylated ACC peptide tail (Arg^{172} in hACC1 and Arg^{277} in hACC2)

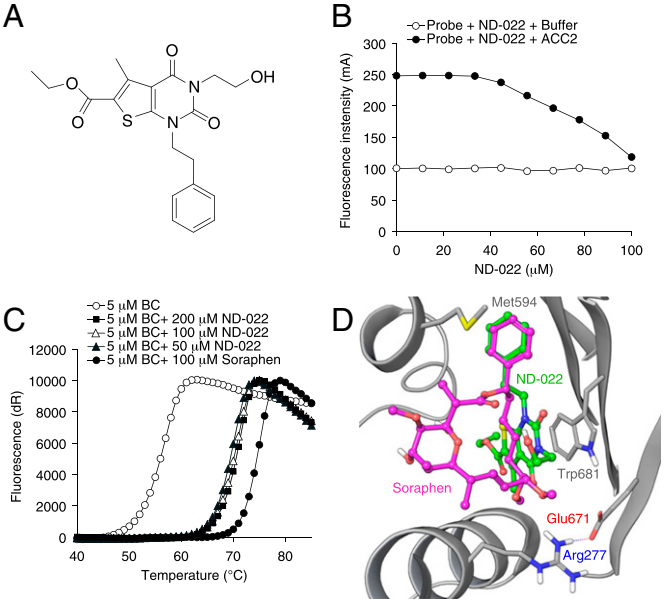

Fig. 1. Mechanism of ACC inhibition by ND-022. (*A*) Chemical structure of ND-022. (*B*) Displacement of Soraphen-TAMARA from hACC2 BC, assessed as a reduction in fluorescence intensity as a function of ND-022. Open circles represent background fluorescence in the absence of hACC2 BC. (*C*) The shift in thermal stability of hACC2 BC in the presence of either Soraphen A or ND-022. The CT domain-binding inhibitor CP-640186, which does not bind to the BC domain of hACC2, did not produce any shift in hACC2 BC thermal stability. (*D*) Cocrystal structure of ND-022 complexed with hACC2 BC overlaid with the structure of hACC2 BC complexed with Soraphen A.

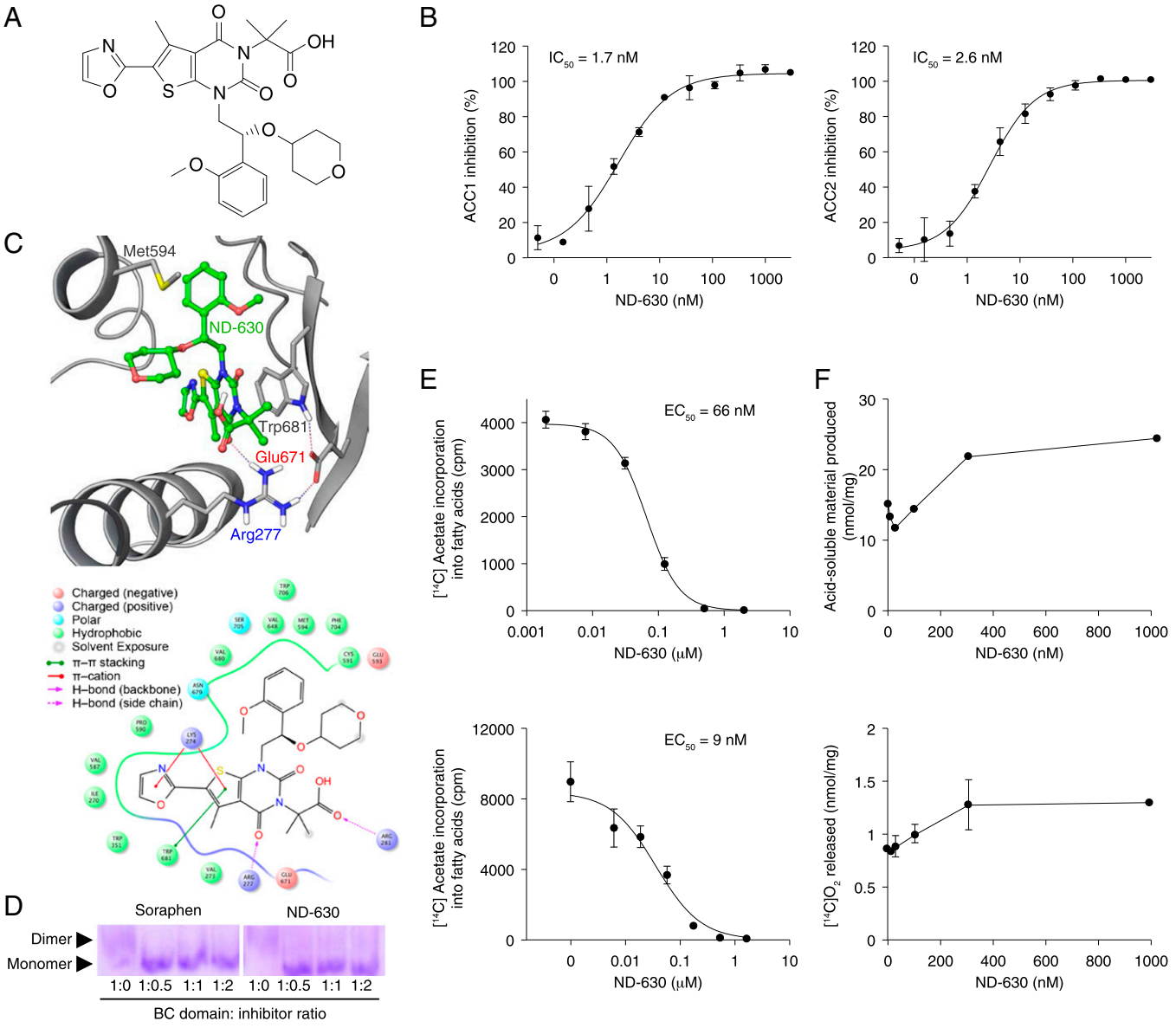

Fig. 2. ACC inhibition by ND-630 in vitro and in cultured cells. (*A*) Chemical structure of ND-630. (*B*) Inhibition (mean ± SD; $n = 3$) of hACC1 (*Left*) and hACC2 (*Right*) as a function of ND-630. (*C, Upper*) Structure of ND-630 modeled into the cocrystal structure of ND-646 (the primary amide of ND-630) complexed with hACC2 BC. (*Lower*) The nature of the amino acid residues interacting with ND-630 in the hACC2 BC dimerization site. (*D*) Coomassie blue-stained nondenaturing 12% polyacrylamide gel (pH 8.8) of hACC2 BC incubated in the absence and presence of a 1:2, 1:1, and 2:1 mol ratio of Soraphen A or ND-630. Arrowheads indicate the migration of hACC2 BC monomer and dimer. (*E*) [^{14}C]Acetate incorporation into fatty acids (mean ± SD; $n = 3$) in HepG2 cells cultured in medium containing 10% FBS (*Upper*) or serum-free medium (*Lower*) as a function of ND-630. (*F*) [^{14}C]Palmitate oxidation by C2C12 cells (mean ± difference of the mean; $n = 2$), assessed by [^{14}C]acid-soluble materials produced (*Upper*) or [^{14}C]O_2 released (*Lower*) as a function of ND-630.

to disrupt subunit dimerization and inhibit activity (35). Unlike Soraphen A, however, ND-630 gains potency by also filling a narrow, deep pocket near Val^{587} and Tyr^{683} (Fig. 2*C*). The inhibition of ACC dimerization by ND-630 was demonstrated further by evaluating the mobility of hACC2 BC in nondenaturing gels in which the enzyme migrates as a dimer in the absence of ND-630 but as a monomer in its presence (Fig. 2*D*), as was observed for Soraphen A with yeast ACC BC (34).

Efficacy of ND-630 in Cultured Cells. To assess the ability of ND-630 to inhibit FASyn in cultured cells, we evaluated its ability to inhibit [^{14}C]acetate incorporation into fatty acids in human hepatic (HepG2) cells. When ND-630 and [^{14}C]acetate were administered to Hep-G2 cells for 4 h, ND-630 inhibited FASyn with EC_{50} values of 66 nM in cells cultured in medium containing 10% serum and 8.7 nM when assessed in serum-free medium (Fig. 2*E*). Under these conditions, total cell number, cellular protein concentration, and incorporation of [^{14}C]acetate into cholesterol were not altered, indicating that the reduction in FASyn produced by ND-630 was not a consequence of reduced cell viability or of nonspecific metabolic effects.

To assess the ability of ND-630 to stimulate FAOxn in cultured cells, we evaluated its ability to stimulate [^{14}C]palmitate oxidation in mouse muscle (C2C12) cells. When ND-630 and [^{14}C]palmitate were administered to C2C12 cells for 6 h, ND-630 increased both the release of [^{14}C]O_2 and the production of [^{14}C]acid-soluble material (Fig. 2*F*).

Pharmacokinetic and Toxicological Properties of ND-630. As a prelude to evaluating the in vivo efficacy of ND-630, we evaluated

its physiochemical, pharmacokinetic, and toxicological properties. ND-630 exhibited an aqueous solubility of 594 μM and human and rat plasma protein binding of 98.5% and 98.6%, respectively. Pharmacokinetic evaluation of ND-630 in male Sprague–Dawley rats [i.v. 3 mg/kg; orally (p.o.) 10 mg/kg] yielded a plasma $t_{1/2}$ of 4.5 h, bioavailability of 37%, clearance (Cl) of 33 mL/min/kg, volume of distribution (V_{dss}) of 1.9 L/kg, oral time of maximum plasma concentration (T_{max}) of 0.25 h, oral area under the curve from 0 to infinity ($AUC_{0-\infty}$) of 1,932 ng·h·mL^{-1}, oral maximum concentration (C_{max}) in the plasma [$C_{max(plasma)}$] of 6.0 μM, in the liver [$C_{max(liver)}$] of 81 μM, and in the quadriceps [$C_{max(quadriceps)}$] of 0.6 μM, and a liver:plasma:quadriceps exposure ratio at T_{max} of 135:10:1. ND-630 does not cross the blood–brain barrier.

In a study to determine the maximum tolerated dose of ND-630, groups of six male Sprague–Dawley rats were given a single oral dose of ND-630 at 100, 300, or 1,000 mg/kg. There were no statistically significant differences in group mean body weight and no adverse ND-630 related effects on hematology, coagulation, or clinical chemistry parameters at any of these doses.

To evaluate toxicities of ND-630 after repeat oral dosing, groups of 10 male and 10 female Sprague–Dawley rats were given ND-630 by oral gavage once daily (QD) for 28 d at doses up to 60 mg·kg^{-1}·d^{-1} (428 times the Sprague–Dawley rat FASyn inhibition ED_{50}). No ND-630–related clinical signs and no changes in body weight, food consumption, hematology, coagulation, or clinical chemistries were observed. Importantly, there were no toxicologically significant findings in clinical chemistry associated with liver, kidney, or muscle integrity or function (Table S3). Furthermore, no mortality was observed, and no target organs of toxicity were identified. Thus, 28-d treatment with ND-630 QD was well tolerated in male and female rats at the highest dose studied.

To determine the effects of ND-630 on the cardiovascular system, ECGs were performed on groups of four male and four female Beagle dogs, once at pretreatment and again at T_{max} (1–4 h post dose) after 1 d and after 4 wk of treatment. ECG tracings were obtained using leads I, II, III, aVR, aVL, and aVF. All dogs maintained sinus rhythms throughout the study. There were no ND-630–related effects on dog ECG rhythms or measurements in this study, and no statistically significant differences were detected between vehicle control and ND-630–treated animals at 100 mg·kg^{-1}·d^{-1} in heart rate, RR interval, PR interval, QRS duration, or QT/QTc interval (Table S4).

Acute in Vivo Efficacy of ND-630. To demonstrate the potential for ND-630 to exhibit chronic in vivo efficacy, we evaluated its ability to reduce acutely malonyl-CoA in the liver and in three skeletal muscles of rats: the soleus, which contains primarily type 1 slow-twitch oxidative fibers, the extensor digitorum longus (EDL), which contains primarily type II fast-twitch glycolytic fibers, and the gastrocnemius, which contains both fiber types (38). When chow-fed male Sprague–Dawley rats were treated orally with ND-630 for 1 h and hepatic and muscle tissues were assessed for malonyl-CoA, hepatic malonyl-CoA was dose-dependently reduced with an ED_{50} of 0.8 mg/kg (Fig. 3*A*). Muscle malonyl-CoA also was reduced dose-dependently (ED_{50} 3–10 mg/kg) (Fig. 3*C*).

Consistent with the acute reduction in hepatic malonyl-CoA, ND-630 reduced hepatic FASyn. When chow-fed male Sprague–Dawley rats treated orally with ND-630 for 1 h were given an i.p. bolus of [^{14}C]acetate and FASyn was assessed 1 h later, ND-630 reduced hepatic FASyn with an ED_{50} of 0.14 mg/kg (Fig. 3*B*). Consistent with the acute reduction in skeletal muscle malonyl-CoA, ND-630 increased whole-body FAOxn, assessed as a reduction in respiratory quotient (RQ). When male Sprague–Dawley rats fed a high-carbohydrate diet were treated with ND-630 and the RQ was monitored, ND-630 reduced the RQ dose-dependently (Fig. 3*D*).

Chronic in Vivo Efficacy of ND-630 in Rats with DIO. To determine the metabolic consequences of chronic ND-630 administration, we studied its actions in two different rat models of DIO. In the first model we fed rats a high-sucrose diet (HSD; AIN76A) for 4 wk before compound administration to induce MetSyn. In this model, the obese phenotype is dependent on the conversion of carbohydrate to fat, and therefore the model explores the ability of FASyn inhibition by ND-630 to affect the phenotype. In the second model we fed rats a high-fat diet (HFD; D12492) for 4 wk before compound administration to induce MetSyn. In this model, the obese phenotype is dependent on the consumption of dietary fat, and therefore the model explores the ability of FAOxn stimulation by ND-630 to affect the phenotype.

Male Sprague–Dawley rats fed an HSD for 4 wk developed the expected phenotype, becoming obese, steatorreic, hyperinsulinemic, insulin-resistant (but not hyperglycemic), hyperleptinemic, hypertriglyceridemic, and hypercholesterolemic. Rats that continued to receive an HSD and in addition were given ND-630 by oral gavage QD for an additional 4 wk (see Table S5 for tissue drug levels) showed a time-dependent reduction in body weight gain relative to the vehicle-treated DIO control group, reducing cumulative body weight gain by up to 20% without altering food consumption (Fig. 4*A*). These results indicate that the effects of ND-630 on body weight and on the parameters described below were not a consequence of caloric restriction. Furthermore, ND-630 dose-dependently reduced the elevated plasma leptin produced by the HSD, with the plasma leptin of the highest treatment groups normalized to that of chow-fed control levels within 1 wk of treatment (Fig. 4*B*). These results indicate that the reduction in body weight was likely caused by a reduction in body fat.

As a consequence of FASyn inhibition and FAOxn stimulation, ND-630 dose-dependently reduced the hepatic steatosis produced by the HSD without altering either hepatic cholesterol or glycogen (Fig. 4*C*). ND-630 also dose-dependently reduced the elevated plasma triglycerides and free fatty acids produced by the HSD (Fig. 4*D*), with normalization to chow-fed control levels within 1 wk. However, plasma glycerol was not altered. ND-630 also increased plasma ketones relative to those in DIO controls, consistent with the increased FAOxn produced by the compound (Fig. 4*E*). ND-630 also markedly reduced plasma cholesterol relative to levels in DIO controls at all doses evaluated (Fig. 4*F*).

As anticipated, because rats fed the HSD remain normoglycemic even though they become insulin resistant and hyperinsulinemic, there were no differences in post-feeding plasma glucose between DIO control and drug-treated groups (Fig. 4*G*). There also were no differences in post-feeding plasma insulin or insulin C-peptide among these groups. However, the 4-wk HSD run-in produced the expected reduction in insulin sensitivity, as noted by a greater insulin excursion, insulin AUC, and glucose AUC in the DIO control group than in the chow-fed control group, as demonstrated in an oral glucose tolerance test (oGTT) (Fig. 4*H*). All dose levels of ND-630 reduced the insulin excursion, insulin AUC, and glucose excursion of the DIO control group, with normalization of the insulin AUC to chow-fed control levels at the highest dose (Fig. 4*H*).

Male Sprague–Dawley rats fed the HFD for 4 wk developed a phenotype similar to that produced by the HSD. In rats that continued to receive the HFD, ND-630 given by oral gavage QD for an additional 2 wk (see Table S6 for tissue drug levels) showed efficacy similar to that produced by ND-630 in HSD rats, but with subtle differences: ND-630 reduced the cumulative weight gain by up to 26% without affecting food consumption (Fig. 5*A*), reduced the hyperleptinemia (Fig. 5*B*), reduced the hyperinsulinemia without altering plasma glucose (Fig. 5*C*), reduced the hepatic steatosis with normalization of hepatic triglycerides at the highest dose (Fig. 5*D*), and reduced the elevated hepatic cholesterol (Fig. 5*E*) without altering plasma triglycerides or plasma cholesterol. Likewise, ND-630 improved insulin sensitivity, as evidenced by reduced insulin excursion and AUC without significant differences in glucose excursion or AUC in an i.p. glucose tolerance test (ipGTT) (Fig. 5*F*).

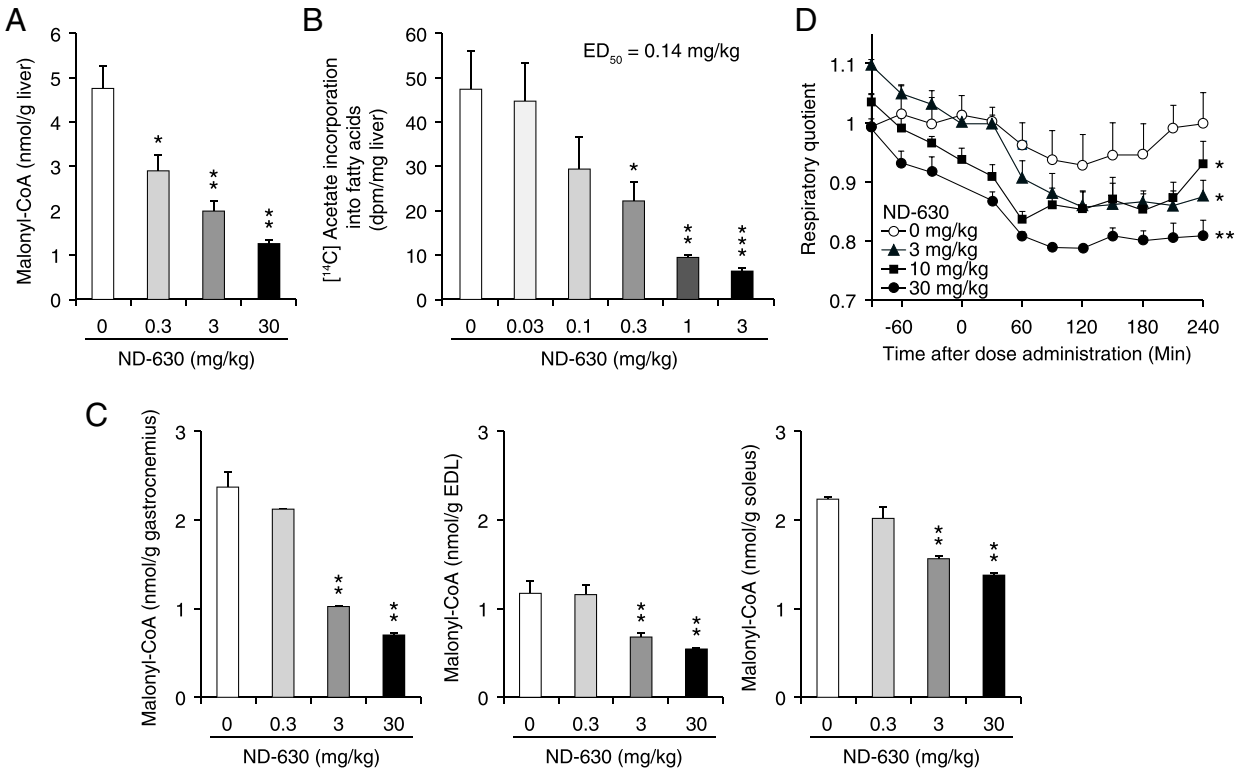

Fig. 3. Acute in vivo efficacy of ND-630 in rats. (*A* and *C*) Chow-fed male Sprague–Dawley rats ($n = 6$ per group) were treated orally with ND-630 for 1 h, and hepatic and skeletal muscle tissues were removed and assessed for malonyl-CoA. (*A*) Hepatic malonyl-CoA (mean ± SD) as a function of ND-630 dose. (*C*) Gastrocnemius (*Left*), EDL (*Center*), and soleus (*Right*) muscle malonyl-CoA (mean ± SD) as a function of ND-630 dose. (*B*) Chow-fed male Sprague–Dawley rats ($n = 6$ per group) were treated p.o. with ND-630 for 1 h. Animals then were given an i.p. bolus of [^{14}C]acetate, and 1 h later liver tissue was removed and fatty acids were extracted and assessed for radioactivity. Shown is the incorporation of [^{14}C]acetate into fatty acids (mean ± SD) as a function of ND-630 dose. (*D*) Male Sprague–Dawley rats fed a high-carbohydrate diet ($n = 4$ per group) were placed individually into Oxymax indirect calorimeter chambers, and RQ was measured every 30 min for 2 h. Animals then were removed from their chambers, given ND-630 by oral gavage, returned to their chambers, and RQ was monitored for an additional 4 h. Shown is RQ (mean ± SD) as a function of time after dosing. *$P < 0.05$, **$P < 0.01$, ***$P < 0.001$ relative to vehicle control.

Chronic in Vivo Efficacy of ND-630 in ZDF Rats. To determine the metabolic consequences of chronic ND-630 administration on diabetes development and to determine whether ND-630 could delay disease onset, we studied its actions in ZDF rats as they progressed from prediabetes to overt diabetes. These animals develop prediabetes, characterized by marked hyperinsulinemia, to compensate for their developing insulin resistance, with little to no hyperglycemia, by 7 wk of age (39). The phenotype advances rapidly to overt diabetes, characterized by hypoinsulinemia, as a result of pancreatic β-cell failure and marked hyperglycemia by 10–12 wk of age (39).

Eight-week-old ZDF rats that were severely hyperinsulinemic and markedly insulin-resistant but only mildly hyperglycemic (Fig. 6*A*) were given ND-630 by oral gavage twice daily (b.i.d.) for 37 d (for tissue drug levels see Table S7). During this time period, vehicle-treated animals progressed to overt diabetes, being markedly hyperglycemic by day 7 (Fig. 6*D*) and severely hypoinsulinemic by day 21 of treatment (Fig. 6*A*), consistent with complete pancreatic β-cell failure by 10 wk of age.

ND-630 had no effect on either food consumption or body weight throughout the 37 d of treatment, indicating that the effects of ND-630 on the parameters described below were not caused by caloric restriction or weight loss. However, ND-630 dramatically and dose-dependently reduced hepatic triglycerides by up to 64%, hepatic free fatty acids by up to 60%, and hepatic cholesterol by up to 32% relative to vehicle-treated animals (Fig. 6*B*). As anticipated from its mechanism of action, ND-630 also dose-dependently increased plasma ketones (Fig. 6*C*).

Although vehicle-treated animals progressed to overt diabetes by the third week of treatment (Fig. 6*A*), post-feeding plasma glucose levels were slightly but not significantly lower in all treatment groups at earlier time points when animals had not yet fully decompensated (Fig. 6*D*). Because plasma insulin was not evaluated at these earlier time points, it is unclear whether ND-630 treatment delayed the decline in plasma insulin during this time frame. However, plasma insulin was significantly increased in all ND-630 treatment groups 15 min and 30 min after an oral glucose challenge on day 21 of treatment, with increases of up to 80% observed after 15 min (Fig. 6*E*). A similar increase in glucose-stimulated insulin secretion (GSIS) was not observed in the vehicle-treated animals (Fig. 6*E*), suggesting some degree of β-cell protection by ND-630. Consistent with this improvement in GSIS, plasma glucose levels also were reduced in all ND-630 animals relative to vehicle-treated control animals 30 min after glucose challenge (Fig. 6*E*), although the glucose AUC was reduced only marginally, albeit dose-responsively (Fig. 6*E*).

Nevertheless, this modest improvement in GSIS by ND-630 and subsequent transient improvement in hyperglycemia after glucose challenge led to a dose-dependent 0.9% reduction in hemoglobin A1c (HbA1c) from 10.2 ± 0.3% ($n = 9$; control) to 9.3 ± 0.2% ($n = 9$; 5 mg/kg b.i.d.; $P = 0.029$) by the end of the study (Fig. 6*F* and Table S8). These results suggest that a reduction in postprandial hyperglycemia produced by ND-630 may have been sufficient to impact hemoglobin glycation. Furthermore, because HbA1c is a measure of glycemic control during the 4–6 wk period before assessment, plasma glucose reduction by ND-630 during the initial 2 wk of the study, before animals had fully decompensated, also likely contributed to the HbA1c reduction.

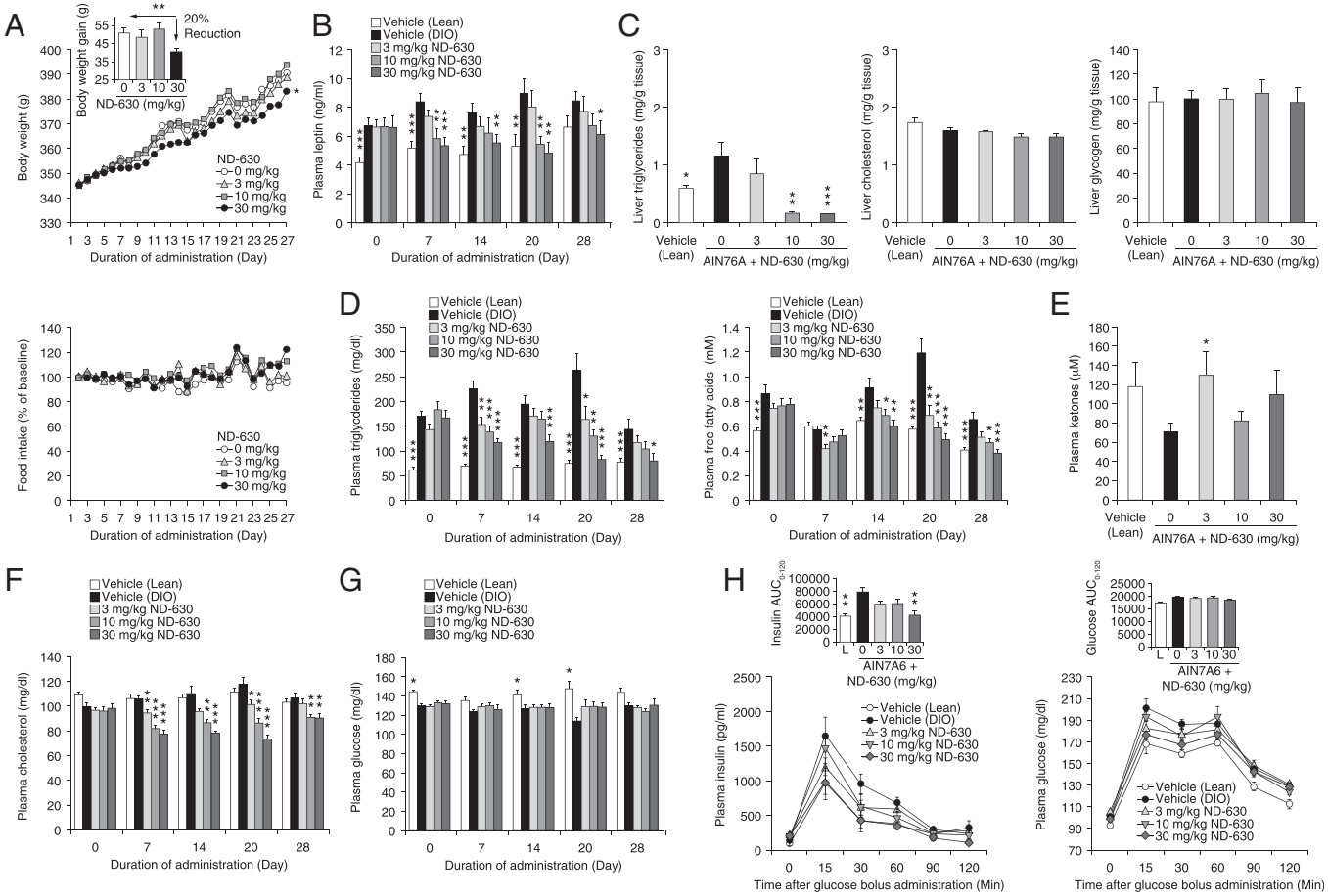

Fig. 4. Chronic in vivo efficacy of ND-630 in rats with HSD-induced obesity. Male Sprague–Dawley rats (n = 14 per group) were fed chow [Vehicle (Lean)] or AIN76A for 4 wk to induce the MetSyn. Rats receiving AIN76A then were given in addition either vehicle [vehicle (DIO)] or ND-630 in vehicle by oral gavage QD for an additional 4 wk. Blood was collected at baseline and weekly, 1 h after dosing, to measure the indicated parameters. After 2 wk of treatment, six animals in each group were killed 1 h after dosing, and hepatic cholesterol and triglycerides were evaluated. After 3 wk of treatment, the remaining animals received an oGTT (2 g/kg glucose). All data are mean ± SEM. (*A*) Body weight (*Upper*) and food consumption (*Lower*) expressed as a function of dosing duration (vehicle, mean lean body weight on day 1 = 267 ± 2.5 g). (*Upper Inset*) Reduction in body weight gain as a function of ND-630 dose. (*B*, *D*, *F*, and *G*) Plasma leptin (*B*), triglycerides (*D*, *Left*) and free fatty acids (*D*, *Right*), cholesterol (*F*), and glucose (*G*) as a function of dosing duration. (*C* and *E*) Liver triglycerides (C, *Left*), cholesterol (*C*, *Center*), and glycogen (*C*, *Right*) and plasma ketones (*E*) on day 28 as a function of ND-630 dose. (*H*) Plasma insulin (*Left*) and glucose (*Right*) as a function of time after glucose bolus administration. (*Insets*) Insulin AUC (*Left*) and glucose AUC (*Right*) as a function of ND-630 dose. $^*P < 0.05$, $^{**}P < 0.01$, $^{***}P < 0.001$ relative to vehicle-treated DIO rats.

Discussion

In this report we describe the discovery and characterization of ND-630, a potent, highly specific, isozyme-nonselective, allosteric, protein–protein interaction ACC inhibitor that interacts within the phosphopeptide-acceptor and subunit dimerization site on the BC domain of both ACC1 and ACC2 to prevent dimerization and inhibit enzymatic activity. As a consequence of this interaction, ND-630 reduces FASyn and stimulates FAOxn in cultured cells and in rats through a mechanism that is functionally identical to the mechanism by which reversible phosphorylation of ACC by AMPK prevents dimerization and inhibits enzymatic activity. In this report we also describe the actions of ND-630 in two distinct models of DIO, one driven by dietary fat and one driven by dietary carbohydrates, demonstrating the ability of ND-630 to reduce the hepatic steatosis, hypertriglyceridemia, hypercholesterolemia, hyperinsulinemia, and hyperleptinemia, improve the insulin resistance, and reduce the weight gain associated with the MetSyn phenotype in these animals. We further describe the ability of ND-630 to delay the progression of prediabetes to overt diabetes in ZDF rats to some degree and to partially preserve GSIS, as glycemic control in these animals deteriorates. Together, these results suggest that ND-630 has the potential to affect favorably a multitude of metabolic disorders, including insulin resistance, dyslipidemia, obesity, MetSyn, and NAFLD, that can lead to the development of T2DM, NASH, cirrhosis, hepatocellular carcinoma, and atherosclerotic vascular disease.

The studies outlined in this report also address the controversies regarding the importance of modulating ACC activity in controlling intermediary metabolism that have emerged as a consequence of conflicting results obtained in isozyme-specific and/or tissue-specific ACC1 or ACC2 genetic deletion studies. As outlined theoretically (1, 9, 19), and also as demonstrated using ACC1 and ACC2 antisense oligonucleotides (22), the ability to limit FASyn in lipogenic tissues (via ACC1 inhibition) while simultaneously stimulating FAOxn in oxidative tissues (via ACC2 inhibition) is efficaciously superior to the inhibition of either isozyme alone. This increased efficacy supports the concept that the efficacy of an ACC2-selective inhibitor in stimulating FAOxn in liver and muscle would be lessened by compensatory increases in hepatic and adipose FASyn and that the efficacy of an ACC1-selective inhibitor would be lessened by restricting its actions to the inhibition of FASyn in fatty acid synthesizing tissues. In support of this concept, studies in global ACC2-knockout mice that retain a fully functional ACC1 gene locus demonstrated compensatory increases in FASyn that either attenuated (20, 21) or

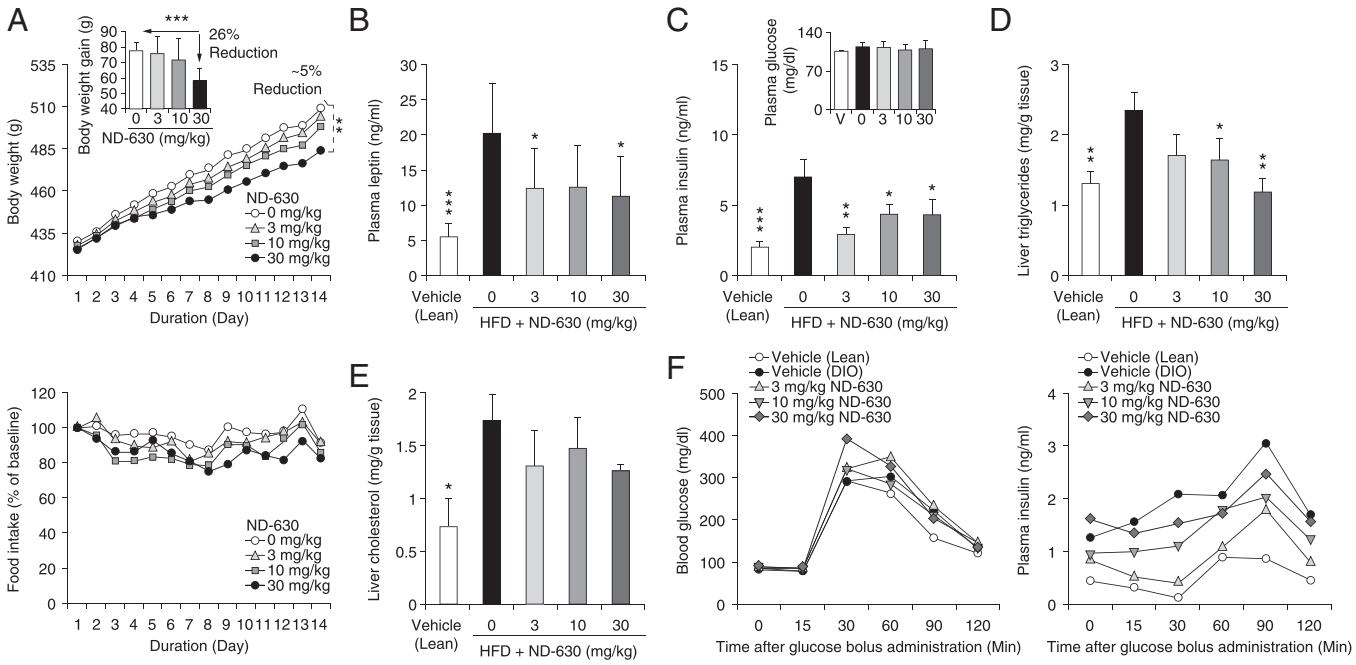

Fig. 5. Chronic in vivo efficacy of ND-630 in rats with HFD-induced obesity. Male Sprague–Dawley rats (n = 6 per group) were fed chow [Vehicle (Lean)] or D12492 for 4 wk to induce the MetSyn. Rats receiving D12492 then were given, in addition, either vehicle [Vehicle (DIO)] or ND-630 in vehicle by oral gavage QD for an additional 2 wk. After 2 wk of treatment, blood was collected 1 h after dosing to measure the indicated parameters. The next morning, after a 12-h fast and 1 h after dosing, animals received an ipGTT (2 g/kg glucose) and then were killed; hepatic cholesterol and triglycerides were evaluated. All data are mean ± SD. (*A*) Body weight (*Upper*) and food consumption (*Lower*) expressed as a function of dosing duration (vehicle lean day 1 mean body weight = 379 ± 27 g). (*Upper Inset*) Reduction in body weight gain as a function of ND-630 dose. (*B–E*) Plasma leptin (*B*), plasma insulin (*C*) and glucose (*C*, *Inset*), liver triglycerides (*D*), and liver cholesterol (*E*) as a function of ND-630 dose. (*F*) Blood glucose (*Left*) and plasma insulin (*Right*) as a function of time after glucose bolus administration. *$P < 0.05$, **$P < 0.01$, ***$P < 0.001$ relative to vehicle DIO.

precluded the demonstration of ACC2 deletion-mediated efficacy (25). Studies in skeletal muscle tissue-specific ACC2-knockout mice also failed to demonstrate any efficacy whatsoever, suggesting that metabolic compensation had limited the impact of ACC2 deletion in these tissue-specific and isozyme-specific knockout animals (26). Similarly, conditional liver-specific ACC1-knockout mice exhibited no reduction in either hepatic malonyl-CoA or in rates of hepatic FASyn as a consequence of compensatory 2.2-fold increases in hepatic ACC2 activity (40). In contrast, our studies clearly demonstrate that simultaneous pharmacologic inhibition of ACC1 and ACC2 results in the reduction of FASyn, stimulation of FAOxn, reduction of hepatic steatosis, improvement in insulin sensitivity, and favorable effects on dyslipidemia in DIO rats fed either the HSD or the HFD and, in addition, results in improvement in GSIS and reduction in HbA1c in ZDF rats.

The studies outlined in this report, in addition to presenting a very safe toxicological profile for ND-630 in 28-d preclinical toxicology studies in rats and dogs, also address hypothetical concerns that the simultaneous inhibition of ACC1 and ACC2 could, in theory, have adverse effects in the various tissues that rely on endogenous FASyn and/or FAOxn. Such tissues include the liver, skeletal muscle, pancreas, and heart (1, 9). For example, many studies have implicated hypothalamic malonyl-CoA in the control of feeding behavior through its actions as a negative regulator of food intake (1, 9), suggesting that reduction in malonyl-CoA in the hypothalamus may increase appetite and partially attenuate the therapeutic effectiveness of ACC inhibition (1, 9). ND-630 does not cross the blood–brain barrier and therefore did not increase food consumption in any animal model evaluated.

It also has been suggested that malonyl-CoA plays an important role in controlling insulin secretion (1, 9) and that reducing pancreatic malonyl-CoA via direct ACC inhibition could attenuate the beneficial effects on GSIS that are induced by the reduction in β-cell fat content mediated by ACC inhibition (1, 9). Although it is generally accepted that this modulation is a key aspect of the normal regulatory machinery that controls insulin secretion in response to changes in plasma glucose and free fatty acids (1, 9), the potential for an ACC1 inhibitor to influence pancreatic malonyl-CoA directly and thereby reduce insulin secretion to a greater extent than might occur via therapeutic improvements in insulin sensitivity theoretically could lead to hyperglycemia even while improving whole-body insulin sensitivity. Such a phenomenon did not occur in the global ACC2-knockout mice (21) that were protected from high carbohydrate diet-mediated hyperglycemia but presumably had normal pancreatic ACC1 activity. In addition, it did not occur in studies in DIO rats fed the HSD and treated with CP-640186 (1, 9, 19), in db/db mice treated with (*S*)-9c (30), or in DIO rats fed either the HSD or the HFD and treated with ND-630. In the DIO rats treated with ND-630 the plasma glucose levels did not change even though insulin sensitivity improved dramatically and, as a normal physiological consequence of this improvement, plasma insulin levels were reduced. Furthermore, ND-630 did not increase hyperglycemia in prediabetic ZDF rats relative to vehicle-treated animals and did not exacerbate the hyperglycemia of overtly diabetic animals but instead improved GSIS and reduced HbA1c levels in these animals. This effect, which also has been reported in db/db mice treated with (*S*)-9c (30), is suggestive of β-cell preservation.

In addition, although ACC inhibition favorably affects cardiac function in the aerobic, triglyceride-laden heart by reducing triglyceride stores that have been associated with depressed contractility, arrhythmias, hypertrophy, and heart failure (1, 9), a variety of reports, mostly from studies in ex vivo working hearts, have suggested that increased FAOxn during and after ischemia may contribute to contractile dysfunction and increase ischemic injury (1, 9). These suggestions have been refuted by studies in rats rendered insulin resistant by HSD feeding, which demonstrate a beneficial effect of FAOxn stimulation on cardiac function during and after ischemia (41). Likewise, studies in

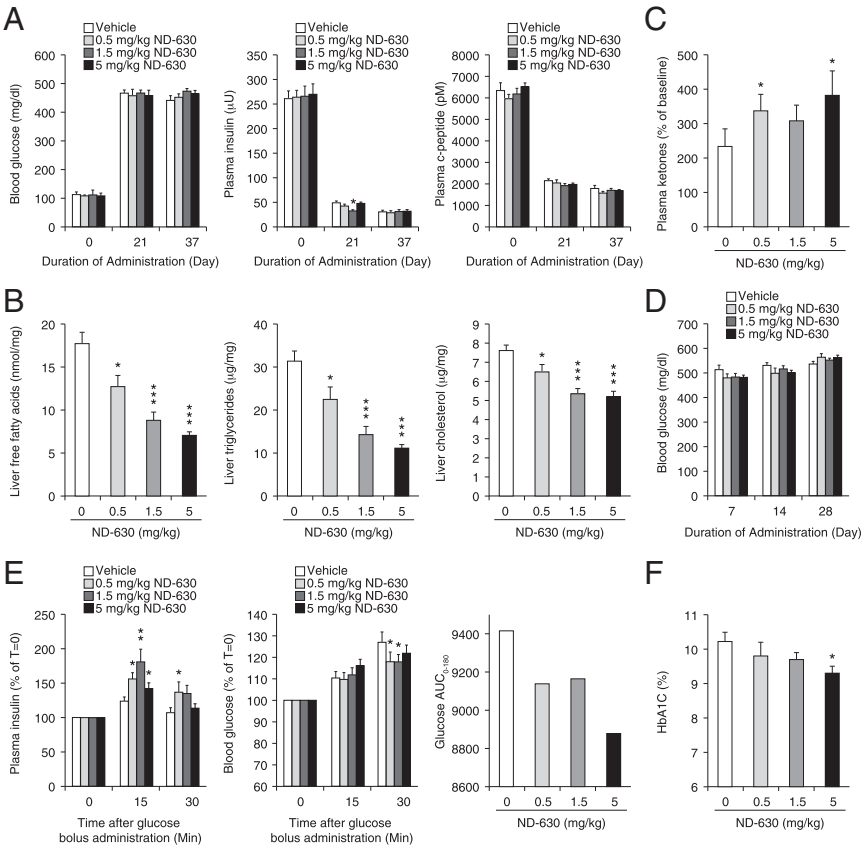

Fig. 6. Chronic in vivo efficacy of ND-630 in ZDF rats. Eight-week-old male ZDF rats ($n = 10$ per group) were given either vehicle or ND-630 in vehicle by oral gavage b.i.d. for 37 d. Blood glucose was measured by glucometer at baseline and weekly just before dosing. Blood was collected at baseline, after 3 wk of treatment, and at the end of the study, 6 h after dosing and after a 6-h fast, for measurement of the indicated parameters. After 3 wk of treatment, animals received an oGTT (1 g/kg glucose). At the end of the study animals were killed, and liver cholesterol, triglycerides, and free fatty acids were determined. All data are mean ± SEM. (*A*) Blood glucose (*Left*), plasma insulin (*Center*), and plasma C-peptide (*Right*) as a function of dosing duration. (*B* and *C*) Liver free fatty acids (*B*, *Left*), triglycerides (*B*, *Center*), and cholesterol (*B*, *Right*), and plasma ketones (*C*) at day 37 as a function of ND-630 dose. (*D*) Blood glucose as a function of dosing duration. (*E*) Plasma insulin (*Left*) and blood glucose (*Center*) as a function of time after glucose bolus administration. (*Right*) Glucose AUC as a function of ND-630 dose. (*F*) HbA1c as a function of ND-630 dose. $*P < 0.05$, $**P < 0.01$, $***P < 0.001$ relative to vehicle control.

cardiac-specific ACC2-knockout mice (42) have shown that the deletion of cardiac ACC2 results in a shift of substrate utilization to FAOxn without negatively impacting cardiac function in the long term and that cardiac ACC2 deletion prevents metabolic reprogramming and sustains myocardial energetics and function in pathological cardiac hypertrophy. In this regard, it is noteworthy that in 28-d rat and dog toxicology studies with ND-630, no adverse cardiac effects were observed at supratherapeutic doses (e.g., 428 times the FASyn inhibition ED_{50}).

Finally, the robust efficacy of ND-630 relative to many of the CT domain-directed ACC inhibitors evaluated in chronic in vivo studies (28) has suggested that the distinct mode of action of ND-630 may offer specific efficacy advantages over CT domain inhibitors of similar affinity. For example, because ND-630 does not inhibit catalytic activity directly but instead inhibits enzyme activity by preventing dimerization, increased substrate and feed-forward activator (citrate) levels that would occur postprandially and also could occur after ACC inhibition itself should have no effect on the inhibitory actions of ND-630, whereas they could attenuate the inhibitory actions of active site-directed CT domain inhibitors. Similarly, the inhibitory actions of ND-630 would not be affected by the reduction in hepatic free fatty acids that occurs after chronic in vivo treatment and that would relieve feedback inhibition by fatty acyl-CoAs to attenuate the actions of CT domain inhibitors, possibly leading to the transient efficacy observed for many of these inhibitors (28). It is more likely, however, that the hydrophilic nature of the dimerization site with which ND-630 interacts facilitates the identification of high-affinity inhibitors that also possess favorable physiochemical and pharmacokinetic properties, whereas the hydrophobic nature of the binding sites with which CT domain inhibitors interact has made the identification of high-affinity inhibitors with favorable pharmaceutical properties more difficult (28).

In conclusion, the results of the studies described in this report offer strong evidence for the safety and utility of isozyme-nonselective ACC inhibition in the treatment of a variety of metabolic diseases. Furthermore, the results of these studies also demonstrate the therapeutic potential of the isozyme-nonselective, allosteric, ACC subunit dimerization inhibitor ND-630 to affect favorably the morbidity and mortality associated with insulin resistance, dyslipidemia, obesity, MetSyn, T2DM, NAFLD, and their sequelae.

Materials and Methods

Measurement of ACC1 and ACC2 Activity and Inhibition. ACC activity was assessed using a luminescent ADP detection assay (ADP-Glo Kinase Assay Kit; Promega) that measures enzymatic activity by quantitating the ADP produced during the enzymatic first half-reaction. Specifically, 4.5 μL of assay buffer containing either recombinant hACC1 (GenBank accession no. NM198834; full length with a C-terminal His-tag, 270 kDa, expressed in Baculovirus-infected Sf9 cell-expression system; BPS Biosciences, catalog no. 50200) or recombinant hACC2 (GenBank accession no. NM001093; full length with C-terminal His-tag, 277 kDa, expressed in a Baculovirus-infected Sf9 cell-expression system; BPS Biosciences catalog no. 50201) were added to the wells of a 384-well Optiplate (PerkinElmer) followed by 0.5 μL of DMSO or DMSO containing inhibitor. Optiplates were incubated at room temperature for 15 min. Then each well received 5.0 μL of substrate mixture to initiate the reaction. Final assay concentrations were 5 nM hACC1 or hACC2, 20 μM ATP, 10 μM (hACC1 assay) or 20 μM (hACC2 assay) acetyl-CoA, 30 mM (hACC1 assay) or 12 mM (hACC2 assay) $NaHCO_3$, 0.01% Brij35, 2 mM DTT, 5% DMSO, inhibitor in half-log increments between 30 μM and 0.0001 μM. After 60-min incubation at room temperature, 10 μL ADP-Glo Reagent was added to terminate the reaction, and plates were incubated at room temperature for 40 min to deplete remaining ATP. Then Kinase Detection Reagent, 20 μL, was added, and plates were incubated for 40 min at room temperature to convert ADP to ATP. ATP was measured via a luciferin/luciferase reaction using a PerkinElmer EnVision 2104 plate reader to assess luminescence.

Expression, Purification, and Crystallization of Recombinant hACC2 BC. A gene encoding hACC2 BC (residues 217–775) was synthesized by Blue Heron Biotechnology and cloned into a modified pET21c (Novagen catalog no. 69742-3) or pET21b (Novagen catalog no. 69741-3) vector encoding an N-terminal hexahistidine tag with a tobacco etch virus (TEV) protease cleavage site and

was overexpressed in *Escherichia coli* BL21 (DE3) Rosetta cells (Transgene catalog no. CD801-03). Protein production was induced with 0.1 mM isopropyl-1-β-D-thiogalactopyranoside (IPTG). Cells were grown overnight at 15–18 °C and harvested by centrifugation. Protein purification is described in *SI Purification of Recombinant hACC2 BC*. Protein crystallization and structure determination are described in *SI Protein Crystallization and Structure Determination*. The data processing and refinement statistics are summarized in Table S9.

Molecular Modeling Techniques. SiteMap v. 2.4 (43) and then WaterMap v. 1.2 (44) were used to determine whether the hACC2 dimerization site contained high-energy hydrations that could be targeted in a virtual screen. We determined that there were two high-energy hydration sites in a deep, narrow pocket near Val^{587} and Tyr^{683} that were accessible from the main soraphen-binding site but were not displaced by Soraphen A. We also noted that additional high-energy hydration sites existed within the hydrophobic pocket with which the alkylphenyl moiety of Soraphen A interacts. We therefore conducted a structure-based virtual screen using commercially available compounds, prepared as 3D models using LigPrep v. 2.4 and Epik v. 2.1 (45), and taking advantage of the standard protocols in GlideXP's Virtual Screening Workflow (VSW/Glide v. 5.6) (46), with an important constraint: During docking, only compounds that hit the high-energy hydration sites in both the deep pocket and the phenyl pocket were advanced.

A ligand-based virtual screen was performed on the same set of compounds using Phase v. 3.2 based on two pharmacophore hypotheses. The first hypothesis was a four-point pharmacophore model built from Soraphen A. The second hypothesis was based on docked poses of the Schrödinger collection of fragments and manual selection of pharmacophore sites with SiteMap and the crystal structure as a guide. Hits from pharmacophore searches using these hypotheses were evaluated using the refinement mode of GlideXP to filter out compounds that cannot fit into the binding pocket. Top-scoring compounds then were docked using GlideXP with the high-energy hydration sites identified by WaterMap as positional constraints.

A combined virtual hit-list of a few thousand compounds was clustered to maximize diversity, and 300 representatives were chosen after visualization of the poses. This process led to the identification of ND-022, which ultimately was confirmed by crystallography to be, to our knowledge, the first synthetic mimic of Soraphen A to interact within the hACC2 dimerization site to inhibit enzymatic activity. Subsequently, lead optimization proceeded rapidly, guided by WaterMap and Prime/MM-GBSA v. 2.2 estimates of binding free energy. From this analysis it was apparent that the 2-ethanol moiety pointed toward the solvent and could be used as an absorption, distribution, metabolism, and excretion (ADME) handle. The proximity of Arg^{281} made carboxylic acids a natural choice to replace ethanol, and gem-dimethylacetic acid was found to provide superior properties. The ethyl ester provided potency to the hit by filling the deep pocket, at the expense of chemical stability, and a search of ester isosteres with MM-GBSA, as well as guidance regarding substituent conformation, sterics, and electronics from quantum chemistry in Jaguar v. 7.7 identified oxazole as a suitable replacement. There also was a clear vector from the phenethyl moiety of ND-022 that corresponded to part of Soraphen's macrocycle leading to its sugar group; a search of a virtual library of chemically accessible substituents quickly established an (*R*)-4-tetrahydropyranyl ether in the sugar-binding pocket as a potent and robust substituent. Finally, WaterMap revealed that the phenyl pocket had a narrow opening toward the solvent, with an extra medium-energy hydration site near the surface capable of being occupied by a 2-methoxy group, further improving potency. Combining these four structure-guided modifications with other chemical features that provided optimal drug-like properties led to the identification of ND-630.

Soraphen Displacement and Thermal Shift Assays. Displacement of fluorescently labeled Soraphen A (Soraphen-TAMARA) from hACC BC by ND-022 was assessed as previously described (47). The protein thermal shift assay for measuring protein thermal stability was conducted as previously described (48), using the environmentally sensitive dye SYPRO Orange with fluorescence data acquired at the end of each 1-min interval using a real-time PCR instrument (Stratagene) which increased the temperature from 25 °C to 100 °C in increments of 1 °C/min.

Preparation of ND-630. 1,4-dihydro-1-[(2*R*)-2-(2-methoxyphenyl)-2-[(tetrahydro-2*H*-pyran-4-yl)oxy]ethyl]-α,α,5-trimethyl-6-(2-oxazolyl)-2,4-dioxo-thieno[2,3-*d*]pyrimidine-3(2*H*)-acetic acid, ND-630, was prepared as described (49).

Measurement of FASyn and FAOxn in Cultured Cells. FASyn was evaluated in HepG2 cells (ATCC catalog no. HB8065) by measuring the incorporation of [2-^{14}C]acetate into cellular lipids (19). FAOxn was assessed in C2C12 cells (ATCC catalog no. CRL1772) by measuring the release of [^{14}C]O_2 and the formation of [^{14}C]acid-soluble materials from [1-^{14}C]palmitate (19, 50).

Studies Using Experimental Animals. All procedures using animals were approved by Nimbus Therapeutics Animal Care and Use Procedures Review Board. Male Sprague–Dawley rats (Charles River Laboratories) were fed chow (Harlan Teklad Rodent Maintenance Diet 2014), an HFD (Research Diets D12492; 60% calories from fat; fat composition 91% lard, 9% soybean oil), or an HSD (AIN76A, Research Diets D10001; 67% calories from carbohydrate; carbohydrate composition 77% sucrose, 23% cornstarch). Male ZDF rats (Charles River Laboratories) were fed chow (Purina 5008). Animals received water ad libitum and were treated orally with 1.0 mL/200 g body weight of either an aqueous saline solution containing 1% Tween 80 and 0.5% methyl cellulose (vehicle) or vehicle containing ND-630.

Rat hepatic FASyn was evaluated by measuring the incorporation of [2-^{14}C]acetate into hepatic lipids (19). Rat hepatic and skeletal muscle malonyl-CoA was measured using a coupled enzymatic assay that uses fatty acid synthase to incorporate one [^{3}H]acetate plus seven malonyl-CoAs into one [^{3}H]palmitic acid molecule (19, 51). Whole-body rat fatty acid utilization was assessed by measuring changes in RQ using an open-circuit, indirect calorimeter (Oxymax; Columbus Instruments) (19).

Male Sprague–Dawley rats (200 g) were fed chow, AIN76A, or D12492 for 4 wk to induce MetSyn. Four days before the end of the diet treatment, animals were acclimated to oral dosing, and baseline food consumption and body weights were determined. At the end of the diet treatment, rats that had received either AIN76A or D12492 were randomized into four treatment groups of 6–14 animals each based on pretreatment body weights. Animals continued to receive AIN76A or D12492 and also were given either vehicle or ND-630 in vehicle by oral gavage QD for up to an additional 4 wk. Body weight and food consumption were monitored daily. Blood was collected on the day before dosing initiation (baseline) and weekly at 1 h after dosing throughout the study to measure the indicated parameters.

For animals receiving AIN76A, after 2 wk of treatment, 6 of the 14 animals in each group were killed 1 h after dosing, and hepatic cholesterol and triglycerides were evaluated. After 3 wk of treatment all remaining animals ($n = 8$ per group) received an oGTT (2 g/kg glucose) after a 12-h fast and 1 h after dosing; blood samples were collected for glucose and insulin assessment just before and 15, 30, 60, 90, and 120 min after oral glucose administration. After 4 wk of treatment, all animals were killed 1 h after final dosing for analysis of drug levels in blood, liver, and quadriceps.

For animals receiving D12492, three of the nine animals in each group were killed after 2 wk of treatment, and blood, liver, and quadriceps samples were analyzed for drug levels. The remaining six animals in each group received an ipGTT (2 g/kg glucose) after a 12-h fast and 1 h after dosing; blood samples were collected for glucose and insulin assessment just before and 15, 30, 60, and 120 min after i.p. glucose administration. Then animals were killed, and hepatic cholesterol and triglycerides were evaluated.

Eight-week-old male ZDF rats (290 g) that were severely hyperinsulinemic and markedly insulin resistant [homeostatic model assessment (HOMA) ∼285] but only mildly hyperglycemic were randomized to four groups of 10 animals each based on glucose, insulin, and HOMA and were given either vehicle or ND-630 in vehicle by oral gavage (b.i.d.) for 37 d. Body weight and food consumption were measured thrice weekly. Blood glucose was measured the day before dosing initiation and weekly from the tail tip by glucometer (Roche) just before dosing. Blood also was collected the day before dosing initiation, after 3 wk of treatment, and at the end of the study (6 h after dosing and after a 6-h fast) for measurement of the indicated parameters. After 3 wk of treatment animals received an oGTT (1 g/kg glucose) after a 6-h fast, and blood samples were collected from the tail tip just before and 15, 30, 60, 90, 120, and 180 min after oral glucose administration for glucose assessment (using a glucometer) and after 15 and 30 min for insulin assessment. At the end of the study animals were killed, and liver cholesterol, triglycerides, and free fatty acids were determined.

Clinical Chemistry. Plasma cholesterol, free fatty acid, total ketone, triglyceride, glycerol, and glucose were measured using the Waco Cholesterol E Kit (catalog no. 439-17501), Waco NEFA-HR(2) kit (catalog no. 999-34691), the Waco Total Ketone Body Autokit (catalog no. 415-73301), the Waco L-Type TG-M Kit (catalog no. 461-08992), the Sigma Glycerol Determination kit (catalog no. FG0100), and the Waco Glucose Autokit C (catalog no. 439-90901). Interassay and intra-assay coefficients of variation for these evaluations were <5%. Plasma insulin, C-peptide, and leptin were determined using the Mercodia Insulin ELISA Rat kit (catalog no. 10-1250-01), the Mercodia C-peptide ELISA Rat kit (catalog no. 10-1172-01), and the ALPCO Diagnostics leptin ELISA kit (catalog no. 22-LEPMS-E01), all with <10% interassay and intra-assay coefficients of variation.

Plasma HbA1c was measured using the HbA1c Enzymatic Assay kit (catalog no. BQ-004-EADD; BQ Kits Inc.).

Hepatic cholesterol and triglycerides were measured as previously described (52). Hepatic glycogen was measured using the Sigma-Aldrich Glycogen Assay kit (catalog no. MAK016).

Statistics. All results are presented as mean ± SEM unless otherwise specified. Results were analyzed using a combination of one-way ANOVA and Dunnett's post hoc analysis, two-way ANOVA with Bonferroni's post hoc analysis, Kruskal–Wallis test with Dunn's post hoc analysis if the variance for each group was statistically different based on Bartlett's test, or one-way ANOVA with repeated measures with Bonferroni's post hoc analysis.

ACKNOWLEDGMENTS. We thank Amanda J. Rogers, Jonathan S. Peters, Jill A. Meyer, Lingling Liu, Miao Chen, Yongliang Jia, Jian Zhao, Katherine Allen, Christopher Hogan, and Benedicte Marcassus for expert technical assistance, Ramy Farid for generating the modeling graphics of Figs. 1*D* and 2*C*, and Eric Smith for producing the final versions of the figures.

1. Harwood HJ, Jr (2005) Treating the metabolic syndrome: Acetyl-CoA carboxylase inhibition. *Expert Opin Ther Targets* 9(2):267–281.
2. Expert Panel on Detection, Evaluation, and Treatment of High Blood Cholesterol in Adults (2001) Executive summary of the third report of the National Cholesterol Education Program (NCEP) Expert Panel on detection, evaluation, and treatment of high blood cholesterol in adults (Adult Treatment Panel III). *JAMA* 285(19):2486–2497.
3. Neuschwander-Tetri BA (2010) Hepatic lipotoxicity and the pathogenesis of nonalcoholic steatohepatitis: The central role of nontriglyceride fatty acid metabolites. *Hepatology* 52(2):774–788.
4. Miller M, et al.; American Heart Association Clinical Lipidology, Thrombosis, and Prevention Committee of the Council on Nutrition, Physical Activity, and Metabolism; Council on Arteriosclerosis, Thrombosis and Vascular Biology; Council on Cardiovascular Nursing; Council on the Kidney in Cardiovascular Disease (2011) Triglycerides and cardiovascular disease: A scientific statement from the American Heart Association. *Circulation* 123(20):2292–2333.
5. Harwood HJ, Jr (2012) The adipocyte as an endocrine organ in the regulation of metabolic homeostasis. *Neuropharmacology* 63(1):57–75.
6. American Diabetes Association (2014) Diagnosis and classification of diabetes mellitus. *Diabetes Care* 37(Suppl 1):S81–S90.
7. Baenke F, Peck B, Miess H, Schulze A (2013) Hooked on fat: The role of lipid synthesis in cancer metabolism and tumour development. *Dis Model Mech* 6(6):1353–1363.
8. Mounier C, Bouraoui L, Rassart E (2014) Lipogenesis in cancer progression (review). *Int J Oncol* 45(2):485–492.
9. Tong L, Harwood HJ, Jr (2006) Acetyl-coenzyme A carboxylases: Versatile targets for drug discovery. *J Cell Biochem* 99(6):1476–1488.
10. Kim KH (1997) Regulation of mammalian acetyl-coenzyme A carboxylase. *Annu Rev Nutr* 17:77–99.
11. Tong L (2005) Acetyl-coenzyme A carboxylase: Crucial metabolic enzyme and attractive target for drug discovery. *Cell Mol Life Sci* 62(16):1784–1803.
12. Brownsey RW, Boone AN, Elliott JE, Kulpa JE, Lee WM (2006) Regulation of acetyl-CoA carboxylase. *Biochem Soc Trans* 34(Pt 2):223–227.
13. Abu-Elheiga L, et al. (2000) The subcellular localization of acetyl-CoA carboxylase 2. *Proc Natl Acad Sci USA* 97(4):1444–1449.
14. Widmer J, et al. (1996) Identification of a second human acetyl-CoA carboxylase gene. *Biochem J* 316(Pt 3):915–922.
15. Bianchi A, et al. (1990) Identification of an isozymic form of acetyl-CoA carboxylase. *J Biol Chem* 265(3):1502–1509.
16. McGarry JD, Brown NF (1997) The mitochondrial carnitine palmitoyltransferase system. From concept to molecular analysis. *Eur J Biochem* 244(1):1–14.
17. McCune SA, Harris RA (1979) Mechanism responsible for 5-(tetradecyloxy)-2-furoic acid inhibition of hepatic lipogenesis. *J Biol Chem* 254(20):10095–10101.
18. Fukuda N, Ontko JA (1984) Interactions between fatty acid synthesis, oxidation, and esterification in the production of triglyceride-rich lipoproteins by the liver. *J Lipid Res* 25(8):831–842.
19. Harwood HJ, Jr, et al. (2003) Isozyme-nonselective N-substituted bipiperidylcarboxamide acetyl-CoA carboxylase inhibitors reduce tissue malonyl-CoA concentrations, inhibit fatty acid synthesis, and increase fatty acid oxidation in cultured cells and in experimental animals. *J Biol Chem* 278(39):37099–37111.
20. Abu-Elheiga L, Matzuk MM, Abo-Hashema KAH, Wakil SJ (2001) Continuous fatty acid oxidation and reduced fat storage in mice lacking acetyl-CoA carboxylase 2. *Science* 291(5513):2613–2616.
21. Abu-Elheiga L, Oh W, Kordari P, Wakil SJ (2003) Acetyl-CoA carboxylase 2 mutant mice are protected against obesity and diabetes induced by high-fat/high-carbohydrate diets. *Proc Natl Acad Sci USA* 100(18):10207–10212.
22. Savage DB, et al. (2006) Reversal of diet-induced hepatic steatosis and hepatic insulin resistance by antisense oligonucleotide inhibitors of acetyl-CoA carboxylases 1 and 2. *J Clin Invest* 116(3):817–824.
23. Qi L, et al. (2006) TRB3 links the E3 ubiquitin ligase COP1 to lipid metabolism. *Science* 312(5781):1763–1766.
24. Fullerton MD, et al. (2013) Single phosphorylation sites in Acc1 and Acc2 regulate lipid homeostasis and the insulin-sensitizing effects of metformin. *Nat Med* 19(12):1649–1654.
25. Hoehn KL, et al. (2010) Acute or chronic upregulation of mitochondrial fatty acid oxidation has no net effect on whole-body energy expenditure or adiposity. *Cell Metab* 11(1):70–76.
26. Olson DP, Pulinilkunnil T, Cline GW, Shulman GI, Lowell BB (2010) Gene knockout of Acc2 has little effect on body weight, fat mass, or food intake. *Proc Natl Acad Sci USA* 107(16):7598–7603.
27. Corbett JW, et al. (2010) Discovery of small molecule isozyme non-specific inhibitors of mammalian acetyl-CoA carboxylase 1 and 2. *Bioorg Med Chem Lett* 20(7):2383–2388.
28. Bourbeau MP, Bartberger MD (2015) Recent advances in the development of acetyl-CoA carboxylase (ACC) inhibitors for the treatment of metabolic disease. *J Med Chem* 58(2):525–536.
29. Griffith DA, et al. (2014) Decreasing the rate of metabolic ketone reduction in the discovery of a clinical acetyl-CoA carboxylase inhibitor for the treatment of diabetes. *J Med Chem* 57(24):10512–10526.
30. Glund S, et al. (2012) Inhibition of acetyl-CoA carboxylase 2 enhances skeletal muscle fatty acid oxidation and improves whole-body glucose homeostasis in *db/db* mice. *Diabetologia* 55(7):2044–2053.
31. Zhang H, Tweel B, Li J, Tong L (2004) Crystal structure of the carboxyltransferase domain of acetyl-coenzyme A carboxylase in complex with CP-640186. *Structure* 12(9):1683–1691.
32. Zhang H, Tweel B, Tong L (2004) Molecular basis for the inhibition of the carboxyltransferase domain of acetyl-coenzyme-A carboxylase by haloxyfop and diclofop. *Proc Natl Acad Sci USA* 101(16):5910–5915.
33. Zhang H, Yang Z, Shen Y, Tong L (2003) Crystal structure of the carboxyltransferase domain of acetyl-coenzyme A carboxylase. *Science* 299(5615):2064–2067.
34. Shen Y, Volrath SL, Weatherly SC, Elich TD, Tong L (2004) A mechanism for the potent inhibition of eukaryotic acetyl-coenzyme A carboxylase by soraphen A, a macrocyclic polyketide natural product. *Mol Cell* 16(6):881–891.
35. Cho YS, et al. (2010) Molecular mechanism for the regulation of human ACC2 through phosphorylation by AMPK. *Biochem Biophys Res Commun* 391(1):187–192.
36. Wei J, Tong L (2015) Crystal structure of the 500-kDa yeast acetyl-CoA carboxylase holoenzyme dimer. *Nature* 526(7575):723–727.
37. Tong L (2013) Structure and function of biotin-dependent carboxylases. *Cell Mol Life Sci* 70(5):863–891.
38. Cornachione AS, Benedini-Elias PC, Polizello JC, Carvalho LC, Mattiello-Sverzut AC (2011) Characterization of fiber types in different muscles of the hindlimb in female weanling and adult Wistar rats. *Acta Histochem Cytochem* 44(2):43–50.
39. Etgen GJ, Oldham BA (2000) Profiling of Zucker diabetic fatty rats in their progression to the overt diabetic state. *Metabolism* 49(5):684–688.
40. Harada N, et al. (2007) Hepatic de novo lipogenesis is present in liver-specific ACC1-deficient mice. *Mol Cell Biol* 27(5):1881–1888.
41. Harmancey R, Vasquez HG, Guthrie PH, Taegtmeyer H (2013) Decreased long-chain fatty acid oxidation impairs postischemic recovery of the insulin-resistant rat heart. *FASEB J* 27(10):3966–3978.
42. Kolwicz SC, Jr, et al. (2012) Cardiac-specific deletion of acetyl CoA carboxylase 2 prevents metabolic remodeling during pressure-overload hypertrophy. *Circ Res* 111(6):728–738.
43. Halgren TA (2009) Identifying and characterizing binding sites and assessing druggability. *J Chem Inf Model* 49(2):377–389.
44. Abel R, Young T, Farid R, Berne BJ, Friesner RA (2008) Role of the active-site solvent in the thermodynamics of factor Xa ligand binding. *J Am Chem Soc* 130(9):2817–2831.
45. Shelley JC, et al. (2007) Epik: A software program for pK_a prediction and protonation state generation for drug-like molecules. *J Comput Aided Mol Des* 21(12):681–691.
46. Friesner RA, et al. (2006) Extra Precision Glide: Docking and scoring incorporating a model of hydrophobic enclosure for protein-ligand complexes. *J Med Chem* 49(21):6177–6196.
47. Raymer B, et al. (2009) Synthesis and characterization of a BODIPY-labeled derivative of Soraphen A that binds to acetyl-CoA carboxylase. *Bioorg Med Chem Lett* 19(10):2804–2807.
48. Vedadi M, et al. (2006) Chemical screening methods to identify ligands that promote protein stability, protein crystallization, and structure determination. *Proc Natl Acad Sci USA* 103(43):15835–15840.
49. Harriman GC, Masse CE, Harwood HJ, Jr, Baht S, Greenwood JR (2013) Acetyl-CoA carboxylase inhibitors and uses thereof. US patent publication US 2013/0123231.
50. Jump DB, Torres-Gonzalez M, Olson LK (2011) Soraphen A, an inhibitor of acetyl CoA carboxylase activity, interferes with fatty acid elongation. *Biochem Pharmacol* 81(5):649–660.
51. Saha AK, Kurowski TG, Colca JR, Ruderman NB (1994) Lipid abnormalities in tissues of the KKAy mouse: Effects of pioglitazone on malonyl-CoA and diacylglycerol. *Am J Physiol* 267(1 Pt 1):E95–E101.
52. Chandler CE, et al. (2003) CP-346086: An MTP inhibitor that lowers plasma cholesterol and triglycerides in experimental animals and in humans. *J Lipid Res* 44(10):1887–1901.
53. Otwinowski Z, Minor W (1997) Processing of X-ray diffraction data collected in oscillation mode. *Methods Enzymol* 276:307–326.
54. Brünger AT, et al. (1998) Crystallography & NMR system: A new software suite for macromolecular structure determination. *Acta Crystallogr D Biol Crystallogr* 54(Pt 5):905–921.
55. Adams PD, et al. (2002) PHENIX: Building new software for automated crystallographic structure determination. *Acta Crystallogr D Biol Crystallogr* 58(Pt 11):1948–1954.
56. Emsley P, Cowtan K (2004) Coot: Model-building tools for molecular graphics. *Acta Crystallogr D Biol Crystallogr* 60(Pt 12 Pt 1):2126–2132.